Chapter 6

Hexagonal to Monoclinic Structural Transformation and Anomalous Luminescent Properties in ZnO and $SrAl_2O_4$ composites

CHAPTER-6
Hexagonal to Monoclinic Structural Transformation and Anomalous Luminescent Properties in ZnO and $SrAl_2O_4$ composites

This chapter, we have studied the evaluation of structure and luminescent properties in ZnO-$SrAl_2O_4$ composite with varying ZnO filler concentration. A set of ZnO(%)-$SrAl_2O_4$ composites are synthesised by varying ZnO concentration from 2.5 % to 20 % through combustion technique, and calcined at 700, 800, 1000 and 1200 ^oC for 3 h. The composites are denoted as SAO(2.5), SAO(5), SAO(10), SAO(15) and SAO(20) for ZnO concentrations 2.5, 5, 10, 15 and 20 %, respectively. The structures and luminescent properties of the composites are compared with the properties of both ZnO and $SrAl_2O_4$. Thermal analysis, microstructural studies, XPS analysis, photoluminescence and thermoluminescence studies of ZnO(%)-$SrAl_2O_4$ composites are discussed in Section 6.1, Section 6.2, Section 6.3, Section 6.4 and Section 6.5, respectively. Section 6.6 gives the summary of results

6.1 Thermal Analysis

Thermal analysis has been employed to find out the phase formation, decomposition and thermal stability of the precursor materials (in gelatinous form) taken to form SAO and SAO-ZnO composite. Fig. 6.1 shows TGA-DTA curves of pristine SAO and the composite of SAO(20). It can be seen from the DTA curve that an endothermic reaction takes place at 134, 157 ^oC accompanied with an exothermic reaction at 145 and 173 ^oC for composite and SAO samples, respectively. This clearly indicates that samples absorb heat for activating the combustion process which releases enormous amount of heat. One may note that the combustion process in composite starts earlier than in SAO. After 200 ^oC in SAO sample, two endothermic peaks could be seen due to the partial and full decomposition of aluminum nitrate. The results are also supported by Capron *et al*. (2002) TGA shows 45 % of weight loss during this decomposition. Two more endothermic peaks associated with almost 10 %

weight loss are found between 550-600 °C. While the first endothermic peak at 588 °C represents the decomposition of strontium nitrate and simultaneous formation of strontium aluminate, the latter one at 631 °C is due to the monoclinic to hexagonal phase transformation of SAO. Such transformation at 650 °C has also been examined by DSC [Douy *et al*. (2003)]. In SAO composite, all endothermic peaks appear similar to SAO with slight changes in their position and intensity. Latter endothermic peak (631 °C) in composite is found to be more intense than SAO and is shifted towards lower temperature. As all the reactions are taken place below 700 °C, therefore we maintain the combustion reaction at 700 °C.

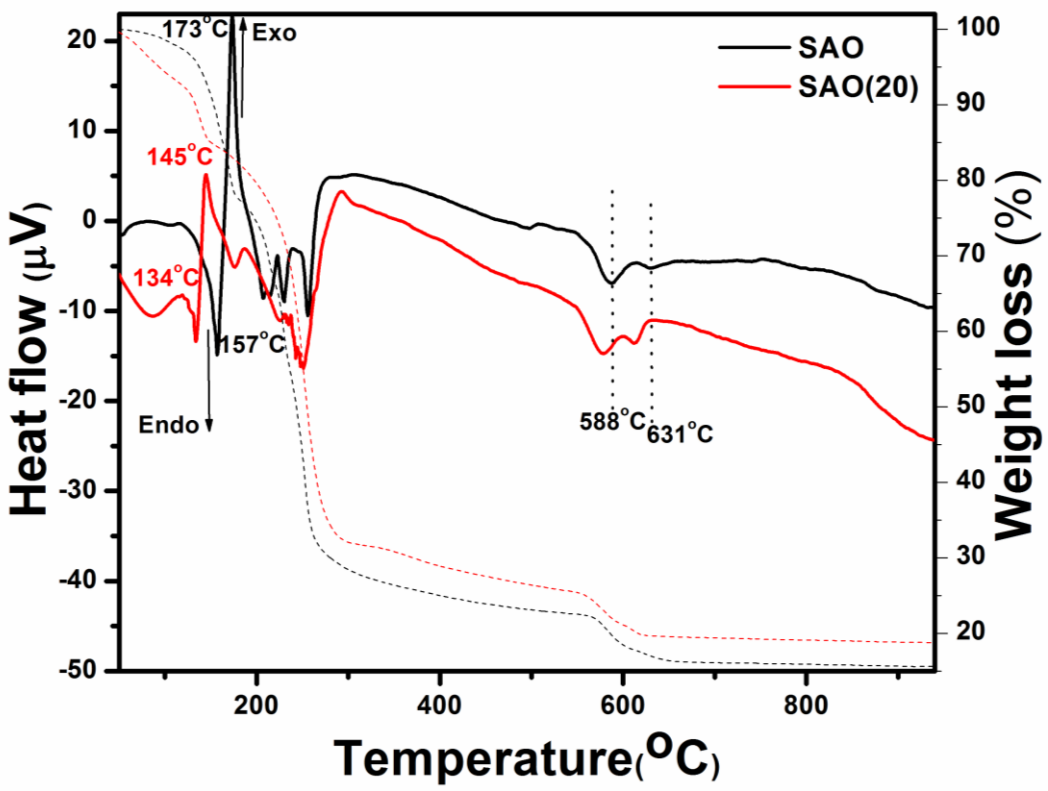

Figure 6.1: TGA-DTA of as prepared SAO and SAO(20) samples measured at 10 °C/min.

6.2 Microstructural Studies

Fig. 6.2 (a-d) shows the SEM images of SAO and SAO(20) composites. SAO calcined at 700 °C shows the presence of large number of pores and demonstrates fluffy nature which could be due to the release of large amount of

N_2, CO_2 gas during combustion. In the sample, we observe 200-300 nm bigger blocks as well as small thin cylindrical rods grown throughout the samples. In the image of 1200 ^oC calcined SAO samples, the blocks clearly turn out into micron sized circular discs and the bigger cylindrical rods are dispersed uniformly throughout sample. The microstructure of SAO(20) composite calcined at 700 ^oC and 1200 ^oC are shown in Fig. 6.2 (c-d) where the former sample is composed of elongated plates or sheets with glassy nature and good dispersity of ZnO in SAO matrix. The large number of micron sized pores are also shown in the inset of (Fig. 6.2 (c)). The particle size of ZnO in SAO(20) composite calcined at 700 ^oC is very small and could not be detected from SEM image. After calcination of SAO(20) at 1200 ^oC, there is a growth of ZnO particles inside the SAO matrix. The ZnO particles larger than 200 nm can be observed in SAO matrix clearly, as shown in the inset of Fig. 6.2 (d).

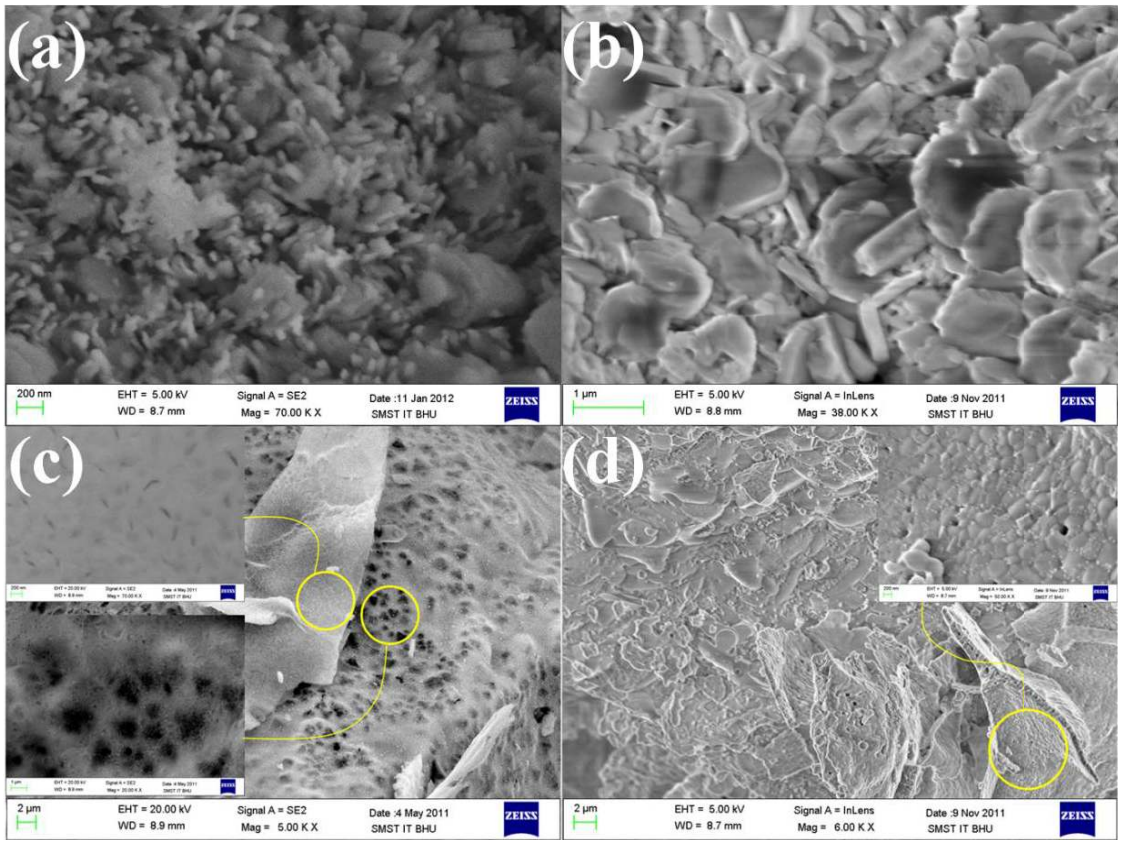

Figure 6.2: SEM image of SAO powder calcined at **(a)** 700 ^oC, **(b)** 1200 ^oC and SAO(20) composite powder calcined at **(c)** 700 ^oC and **(d)** 1200 ^oC.

X-ray diffraction patterns of SAO powder synthesised by combustion method, calcined at 700, 800, 1000 and 1200 °C for 3 hour are shown in Fig. 6.3. It is observed that though the Bragg peaks match with the peaks of standard monoclinic (JCPDS 00-034-0379) phase of SAO, presence of few extra peaks in sample calcined at 700 and 800 °C indicate the incomplete phase formation. Further increasing the calcination temperature to 1000 °C, the XRD peaks match better with the monoclinic ($P2_1$) phase of SAO at the expense of impurity phases. At 1200 °C, no change is observed except sharpening of the peaks. In addition to monoclinic phase of SAO, weak peaks due to $Sr_3Al_2O_4$ which is the secondary phase of $SrO\text{-}Al_2O_3$ phase diagram, remain present even after calcining at 1000 and 1200 °C. Though impurity phases are significantly reduced, we could not remove them completely. In literature, it has been reported that there exists some common secondary phases such as $SrAl_4O_7$, $Sr_3Al_2O_6$ and $Sr_4Al_{14}O_{25}$ of the $SrO\text{-}Al_2O_3$ in the phase diagram which generally

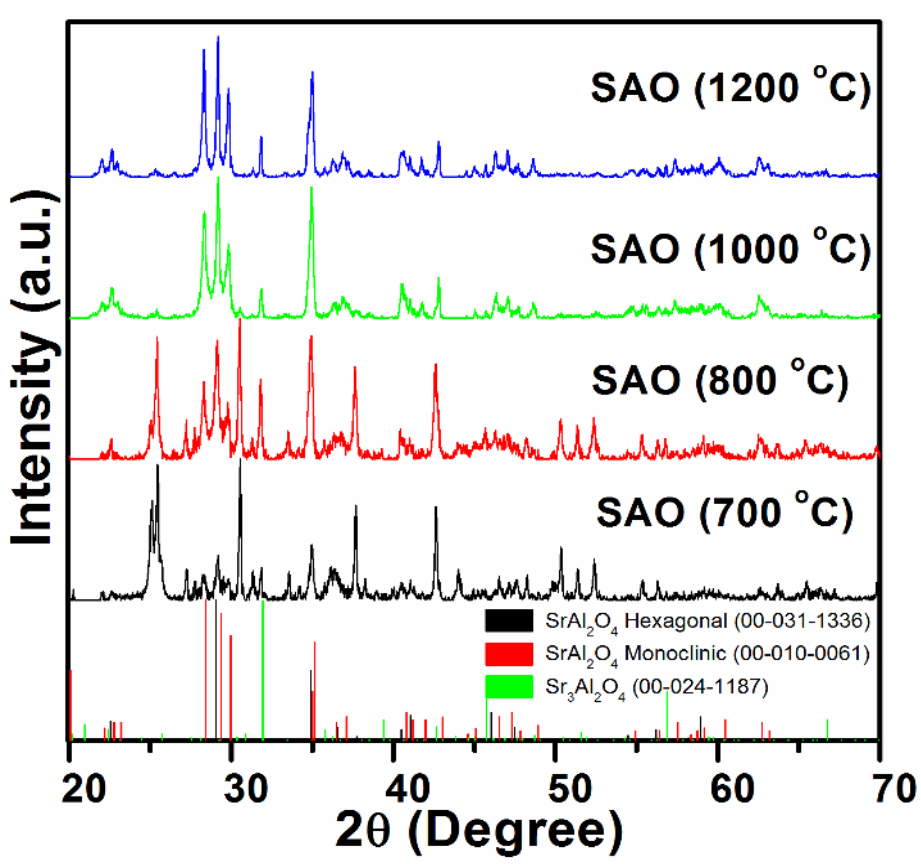

Figure 6.3: Normalised XRD patterns of SAO sample calcined at different temperatures in the range of 700–1200°C.

exists with SAO and difficult to remove. For example, Escribano *et al.* (2005) could not suppress the secondary phase of $Sr_3Al_2O_6$ even after calcination at 1400 ^oC/10h. Different methods have been adopted by different authors to grow pure phase of SAO and/or to reduce the secondary phases present in SAO either by doping or by calcining at different temperatures. Jung *et al*. (2006) have shown that by doping boron, the monoclinic phase is obtained without undesired secondary phases at lower temperature. It has been thought that boron replaces Al(III) ions and generates distortions in the Al-framework, so that it could lead to a decrease in the processing temperature of SAO [Escribano *et al*. (2005)]. However, at higher calcination temperature (>1300 ^oC), impurity of $Sr_4Al_{14}O_{25}$ phase is found to be present which is the major drawback of boron doping. According to Nag and Kutty (2003), the formation of $Sr_4Al_{14}O_{25}$ is due to the reaction of B_2O_3 and SAO which leads another impure phase of $SrAl_2B_2O_7$. Zheng *et al*. (2011) have reported that PVP in PVP-SAO composite favours the formation of SAO phase and prevents the formation of $SrAl_4O_7$ impurity phase to a certain extent. We have been able to reduce the secondary phase significantly using ZnO-SAO composite even at 700 ^oC without any doping. The X-ray diffraction pattern of ZnO-SAO composites with varying ZnO percentage (0 to 20 %) calcined at 700 ^oC are shown in Fig. 6.4. The ZnO peaks present in the spectra are marked by '*'. While, incomplete phase formation is observed in SAO(0), monoclinic phase as major phase in addition with the other minor phases has been observed in SAO(2.5) sample. As we increase the ZnO content, both monoclinic and hexagonal phases of SAO coexist upto ZnO concentration approaches 15%. In SAO(20), monoclinic phase almost transforms to hexagonal phase. X-ray diffraction pattern of ZnO-SAO composites with varying ZnO percentage (0 to 20 %) and calcined at 1200 ^oC are shown in Fig. 6.5. In addition to ZnO, all the Bragg peaks of monoclinic SAO are found present in all ZnO-SAO composites. The intensity of all the peaks related to ZnO are found in well scale with ZnO concentration in ZnO-SAO composites. We have studied the phase change of

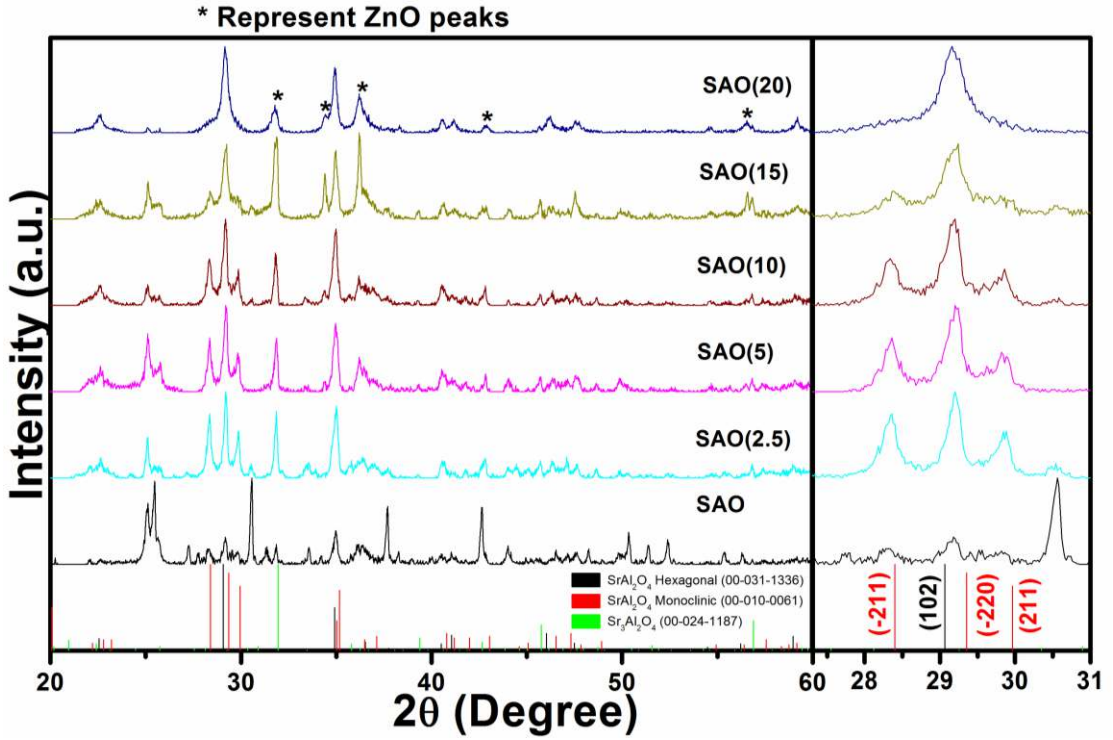

Figure 6.4: Normalised XRD patterns of SAO, SAO(2.5), SAO(5), SAO(10), SAO(15) and SAO(20) composites calcined at 700 ^{o}C.

.

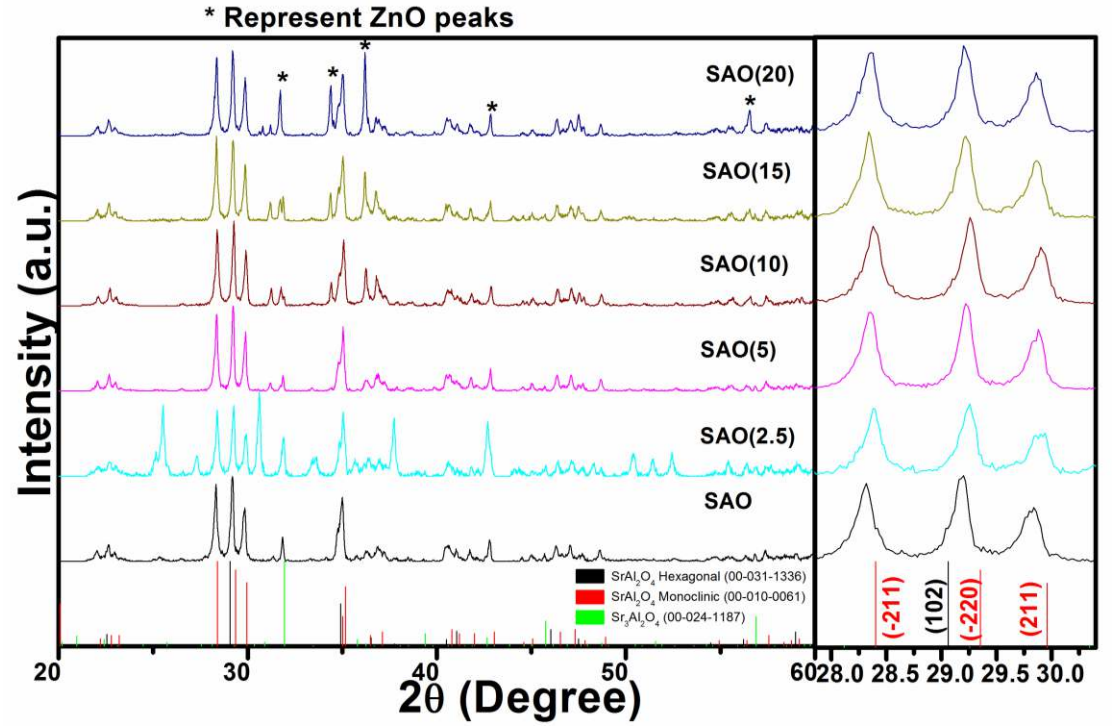

Figure 6.5: Normalised XRD patterns of SAO, SAO(2.5), SAO(5), SAO(10), SAO(15) and SAO(20) composites calcined at 1200 ^{o}C.

SAO(20) composite, after calcining the sample at two more intermediate temperature 800 and 1000 ^{o}C. The X-ray diffraction patterns of calcined SAO(20) composites from 700 to 1200 ^{o}C are depicted in Fig. 6.6. The Bragg peaks are found to be well matched with the wurtzite structure of ZnO (JCPDS 89-1397) as well as with the hexagonal phase ($P6_322$) of SAO (JCPDS 31-1336) after calcined at 700 ^{o}C and 800 ^{o}C. Further, increasing the calcination temperature to 1000 ^{o}C, the hexagonal phase almost converts to monoclinic($P2_1$) phase of SAO. A closer view of evolution of monoclinic to hexagonal phase formation and vice versa are shown in the right side of the XRD spectra depicted in Fig. 6.4 and Fig. 6.6. With increasing ZnO content, (-211), (-220) and (211) peaks of monoclinic phase are merged into (102) peak of hexagonal phase and with increase in calcination temperature of SAO(20) composite to 1000 ^{o}C, the reverse effect is observed (Fig. 6.4 and Fig. 6.6). At 1200 ^{o}C, while the ZnO phase remains unchanged, the monoclinic phase of SAO becomes more pronounced and peak intensities for both ZnO and SAO are enhanced, indicating the growth of the particles. Further, we have fitted the

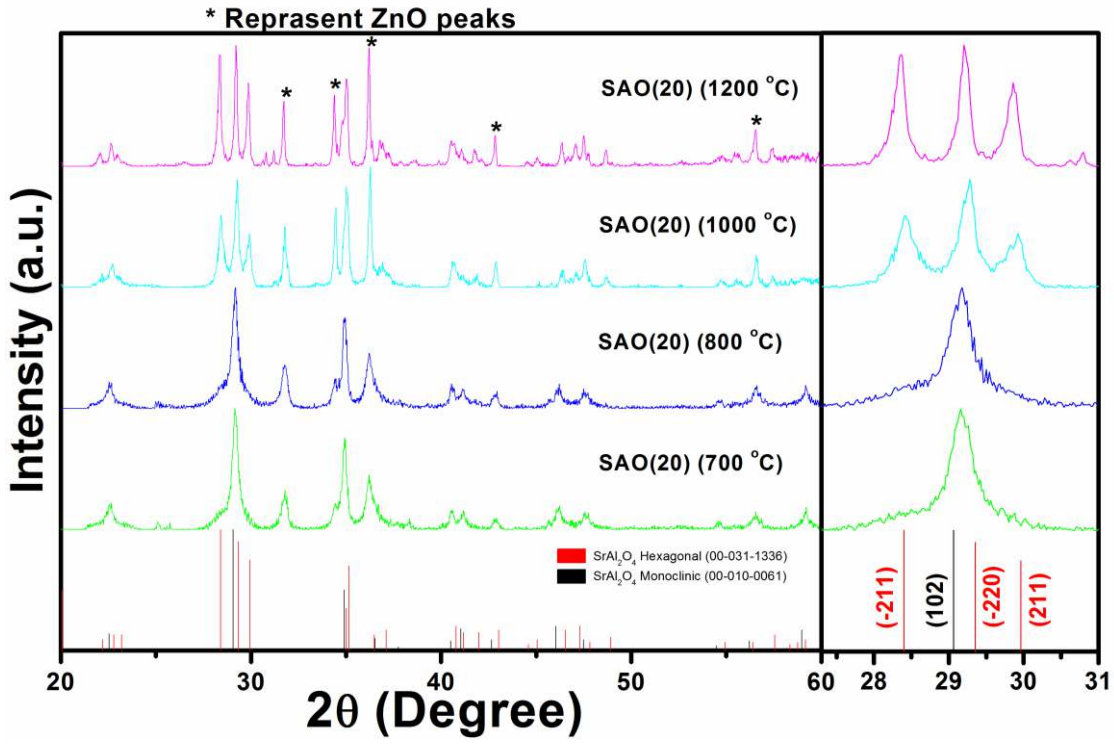

Figure 6.6: Normalised XRD patterns of SAO(20) nanocomposites calcined at different temperatures.

XRD pattern of the composite with Lebail profile fitting using Fullprof program, shown in Fig. 6.7. SAO(20) composite calcined at 800 ^{o}C has been fitted with P6$_3$mc and *P*6$_3$22 space groups corresponding to ZnO and hexagonal phase of SAO, respectively. The composite calcined at 1000 ^{o}C has also been fitted with P6$_3$mc and *P*2$_1$ space group corresponding to ZnO and monoclinic phase of SAO. The lattice parameter and lattice volume of both the samples obtained from fitting are tabulated in Table 6.1. As there is a gradual change in phase with increase in ZnO concentartion and calcination tempertaure, we have, thus estimated the phase fraction from the integral peak area intensity ratio of monoclinic peak (211) to the main peak (-220) or (102) as shown in Fig. 6.8 (a-b). One may clearly observe that with increase in ZnO content, the peak integral area ratio decreases whereas increases with increasing calcination

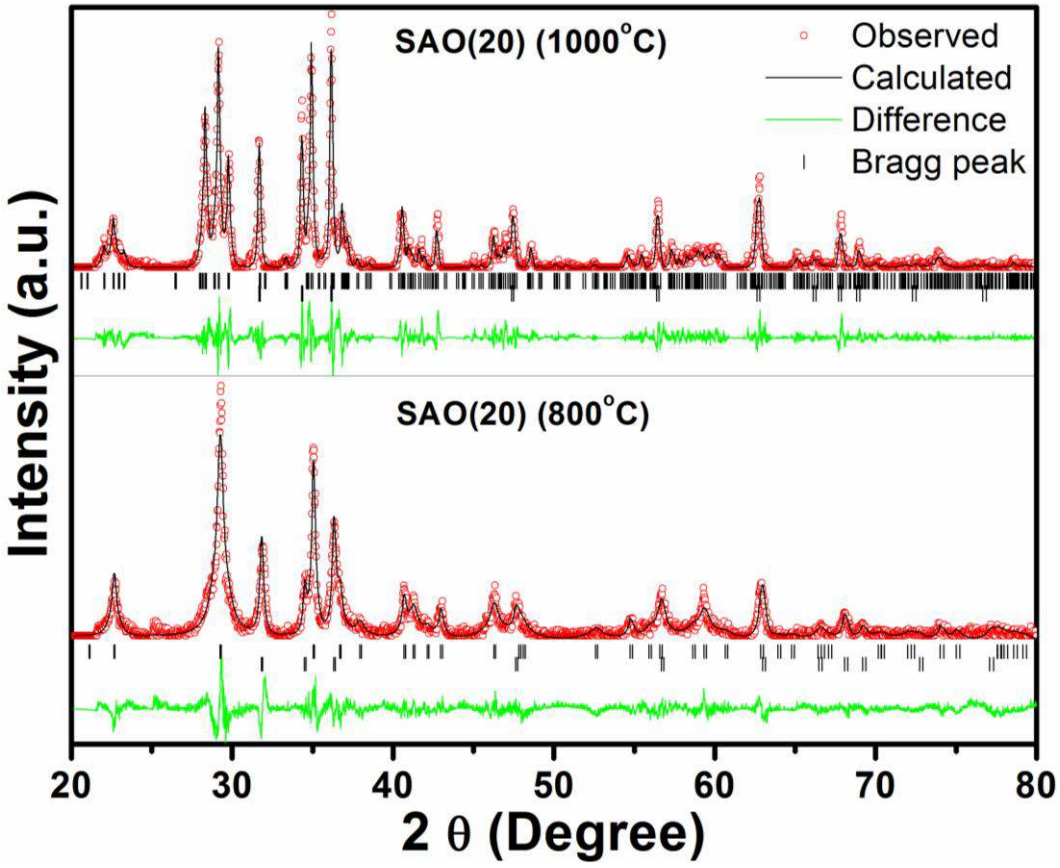

Figure 6.7: The fitted experimental data of XRD using Fullprof program with P6$_3$mc and *P*6$_3$22, and P6$_3$mc and *P*2$_1$, for 800 ^{o}C and 1000 ^{o}C calcined SAO(20) nanocomposites, respectively.

temperature it decreases. While, both monoclinic and hexagonal phase coexists in SAO composite for the ZnO concentration in between 0 % to 15 %, almost pure hexagonal phase is observed in SAO(20) composite. Again, hexagonal phase of SAO(20) composite transforms to monoclinic with increasing the calcination temperature from 700 to 1200 ^{o}C. Stable hexagonal phase of SAO at room temperature in presence of ZnO has not been shown earlier to the best of our knowledge.

Table 6.1 The reported (JCPDS) lattice parameter of monoclinic and hexagonal phase of SAO and wurtzite phase of ZnO compared with the extracted cell parameters after Le-bail profile fitting of SAO(20) composite calcined at 800 and 1000 ^{o}C.

JCPDS Number		Cell Parameters			
		a	b	c	Volume
031-1336	P 6_3 2 2	5.14	5.14	8.46	193.61
034-0379	P 2_1	8.44	8.82	5.16	383.68
089-1397	P 6_3 m c	3.25	3.25	5.21	47.77
SAO(20)	P 6_3 2 2	5.12	5.12	8.41	190.89
800C	P 6_3 m c	3.25	3.25	5.20	47.40
SAO(20)	P 2_1	8.48	8.88	5.18	388.97
1000C	P 6_3 m c	3.26	3.26	5.22	48.10
a, b, and c are in A^o, for above P 2_1($\alpha = \gamma = 90, \beta = 93.216$)					

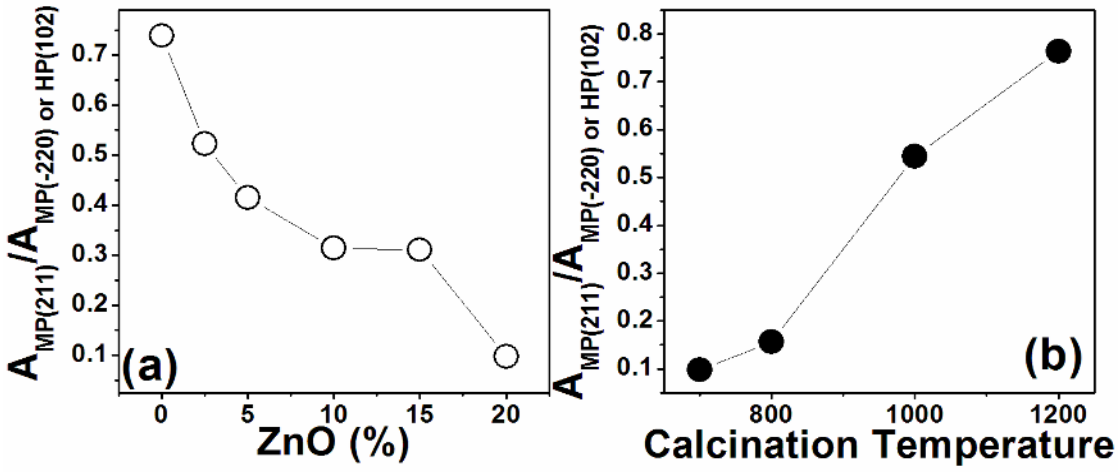

Figure 6.8: The integral peak area ratio of the MP peak (211) to the main peak (-220) or (102) of MP or HP respectively in the XRD patterns of **(a)** ZnO-SAO composite with varying ZnO concentration and calcined at 700 ^{o}C and **(b)** SAO(20) composite with increasing calcination temperature.

There is a general agreement in literature that the degree of deformation of high tridymite type framework in AM_2O_4 derivatives is determined by the size of $[A]^{n+}$ cations with respect to size of cavities in $[M_2O_4]^{n-}$ frame work [Henderson *et al*. (1982); Barbier *et al*. (1988)]. In $SrAl_2O_4$, Sr^{2+} is apparently too small for nine fold coordination of the large cavities in the undistorted $[Al_2O_4]^{2-}$ frame work and the structure at room temperature is severely collapsed to form irregular polyhedral and hence results into monoclinic phase [Schulze *et al*. 1981]. On heating, thermal expansion of 'A' site higher than that of AlO_4 tetrahedra, drives the structure towards the ideal hexagonal symmetry. Furthermore, it has been demonstrated that hexagonal phase formation occurs at room temperature by adding dopants like Ca, Ba and Eu. The smooth change from monoclinic to hexagonal phase has been observed in SAO by substituting Ba (upto 37 at%) in the Sr^{2+} site [Wu *et al*. 2009]. Chen et al. (2006) demonstrate the stabilisation of hexagonal structure in Ca doped SAO with increasing Ca^{2+} concentration from 20 to 50 at%. Shi *et al*. (2004) have shown that 12 % of Eu dopant in SAO shows complete hexagonal phase after synthesising through spray pyrolysis process and annealing in reduced atmosphere. No impurity phases of europium oxide and/or europium aluminates could be detected, further confirming all Eu incorporation into the interstitial space formed by AlO_4 tetrahedra to substitute Sr [Shi *et al*. (2004)]. However, annealing in oxygen atmosphere, the hexagonal phase could not be obtained and monoclinic phase with Eu related impurity phases are found. At the same time, SAO prepared by solid state reaction process, shows impurity phases of europium oxide and/or europium aluminates when Eu concentration approaches 12%. In the former case, the reason behind the hexagonal phase formation is mainly due to the concentration of oxygen defects related to Eu concentration. As long as the concentration of oxygen defects is sufficient, the hexagonal phase remains stable even at room temperature. Similar to Eu doped SAO, we have also observed hexagonal phase in higher concentration of ZnO in SAO. In addition to the formation of monoclinic or hexagonal phase of SAO, we have observed wurtzite phase of ZnO in the composite, irrespective

of the concentration of ZnO. Addition of ZnO in SAO generates two possibilities: one is the replacement of Sr by Zn and the other would be the replacement of Al by Zn. Although the valency of Zn and Sr are same, due to large difference in the ionic radius of Zn^{2+} (0.60 to 0.745A) and Sr^{2+} (1.32A), the nine fold coordination of Zn in the undistorted $[Al_2O_4]^{2-}$ frame work leads to severely collapsed structure at RT and hence, crystallizes in monoclinic structure. If Zn replaces Al, oxygen vacancy is produced which varies with concentration of ZnO. At lowest concentration of ZnO, SAO always shows monoclinic phase at RT which demonstrates that at lower concentration of ZnO, even if Zn replaces Sr and/or Al, the phase of SAO does not change. Therefore, oxygen vacancy formation due to replacement of Al does not play any important role in the phase formation at low concentration of ZnO. With gradual increase in ZnO content in SAO, more and more oxygen vacancies are produced and both monoclinic and hexagonal phases coexist upto 15 % of ZnO composite. At 20 % of ZnO composite, the oxygen vacancies are sufficient enough to stabilize the hexagonal phase. Ultimately, the oxygen vacancies play a crucial role in transformtion of phase from hexagonal to monoclinic and vice versa. It can be easily understood that the oxygen vacancies are filled by calcination at higher temperature in oxygen atmosphere and hence hexagonal phase transforms to monoclinic phase.

6.3 XPS Analysis

For further confirmation of the role of oxygen vacancy, we have carried out the XPS measurement of SAO(2.5), SAO(20) composites calcined at 700 ^{o}C and SAO(20) composite calcined at 1200 ^{o}C. XPS full scan spectra of all these samples are shown in Fig. 6.9(a). Fig. 6.9(b) show the O 1s XPS spectra. All the peaks are calibrated with respect to the carbon 1s peak at 284.6 eV. The O 1s core level shows slightly asymmetric shape which can be fitted well with three curves denoted as curve 1, 2 and 3 using XPSPEAK version 4.1. The difference pattern obtained between the observed and fitted spectrum is shown beneath the XPS spectrum. The three curves show peak positions at 530.3, 531.3 and 532.2 eV for curve 1, 2 and 3, respectively. The peak at 530.3 eV is

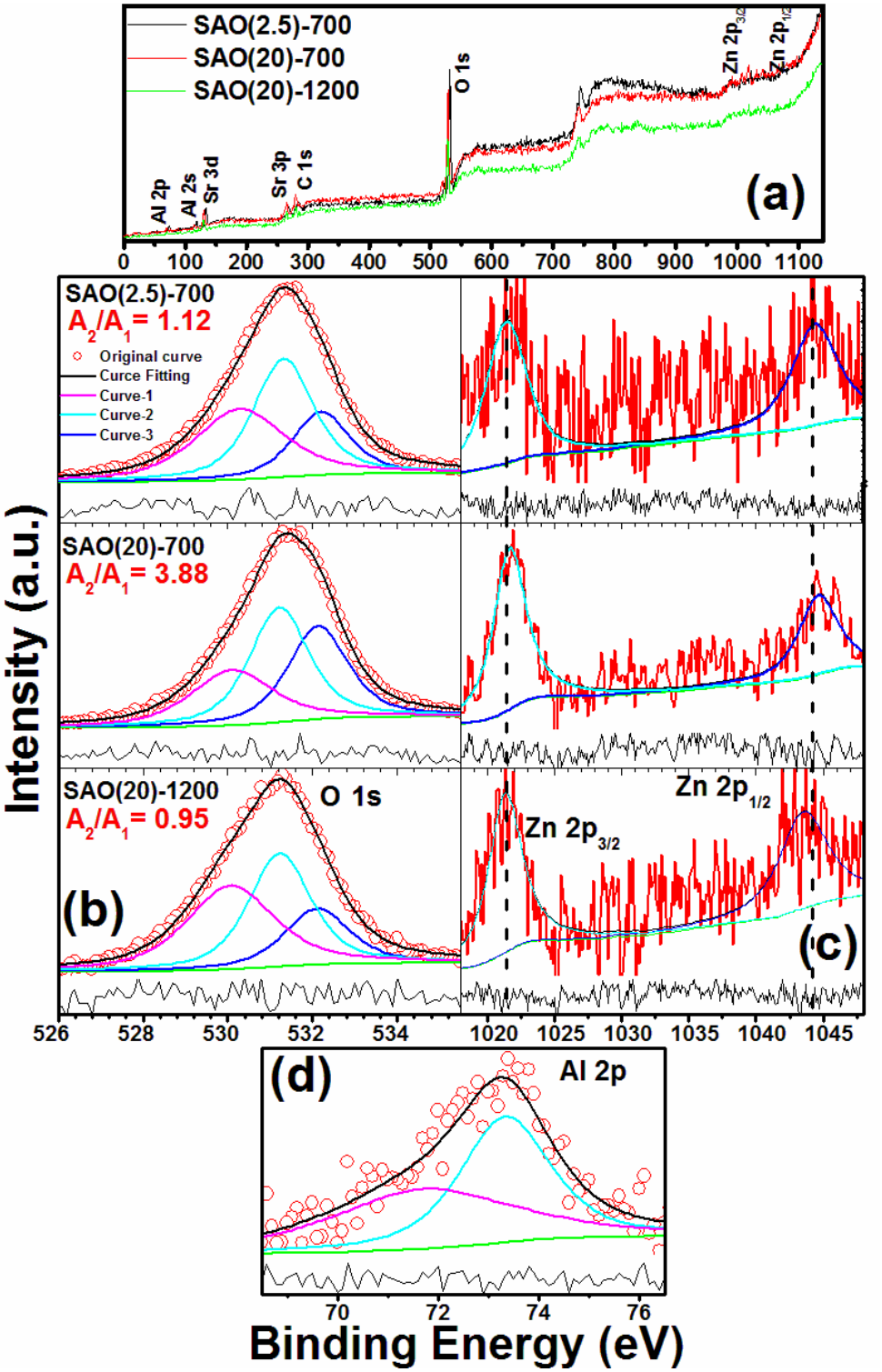

Figure 6.9: The XPS spectra of **(a)** SAO(2.5) and SAO(20) composites calcined at 700 °C and the SAO(20) composite calcined at 1200 °C in full scan, **(b)** O 1s core level spectra deconvoluted into three peaks, **(c)** Zn 2p core level spectra for SAO(2.5) and SAO(20) calcined at 700 °C and SAO (20) calcined at 1200 °C and **(d)** a typical Al 2p spectrum of SAO(20) composite calcined at 1200 °C after deconvolution.

ascribed to the oxygen atoms of SAO, peak at 531.3 eV is attributed to O^{2-} ions in oxygen deficient regions in SAO and the peak around 532.2 eV is assigned to the hydroxyl groups, chemisorbed oxygen and organic oxygen on the surface of the sample [Lin *et al*. (2005); Tam *et al*. (2006); Duan *et al*. (2012); Gesing *et al*. (2012)]. To compare the oxygen vacancies in different samples, the area of the curve 1 and 2 is calculated after deconvolution including the area ratio, A_2/A_1. Comparing A_2/A_1 in SAO(2.5) and SAO(20) calcined at 700 ^oC (Fig. 6.9(b)), it is observed that the area ratio is higher in SAO(20) than in SAO(2.5), indicating the enhancement of oxygen vacancy concentration. Calcining SAO(20) at 700 ^oC and 1200 ^oC, A_2/A_1 is found to decrease again which confirms the decrease in oxygen defect driven phase transformation from hexagonal to monoclinic as observed in XRD spectra. XPS of Zn 2p core level spectra of the same composites are shown in Fig. 6.9(c). The binding energy located at 1021.5 eV and 1044.2 eV are attributed to the $2p_{3/2}$ and $2p_{1/2}$ of Zn ions respectively, which matches with the binding energy of Zn^{2+} ion and does not show any significant change with increasing Zn concentration [Gesing *et al*. (2012); Panigrahy *et al*. (2010)]. A typical Al 2p spectrum is plotted in Fig. 6.9(d) which shows relatively broad and asymmetric shape. The peak at 73.33 eV matches with the Al^{3+} ion. The asymmetric shape indicates more than one coordination environment at Al^{3+} ion in the composite [Gesing *et al*. (2012); Duan *et al*. (2011)].

6.4 Photoluminescence Study

Photoluminescence spectra at room temperature for SAO and SAO composites calcined at different temperatures are shown in Fig. 6.10. One may notice four sharp emission peaks at 420, 650.9, 663.7, 689.8 nm and a broad band in the range of 700-900 nm for pure SAO sample. Calcining SAO at 1200 ^oC the four sharp emission peaks at 420, 650.9, 663.7, 689.8 nm become more pronounced and a shoulder at 800.12 nm appear on the broad band in the range of 700-900 nm. The broad emission of the SAO could be due to the intrinsic defects as has been reported in similar compound by Emen *et al.* (2010) and

Beauger *et al*. (1999). The sharp peaks seem to be the spectral lines of Sr (Beauger *et al*. (1999)]. In SAO(2.5) composite calcined at 700 °C, a sharp emission peak at 384 nm and a broad band (700-900 nm) with shoulder at 800.12 nm is observed. The peak at 384 nm corresponds to the near band edge (NBE) emission of ZnO. Increasing the calcination temperature of SAO(2.5) from 700 to 1200 °C, gradually the shoulder becomes more intense at the expense of NBE of ZnO. In SAO(2.5) composite, all the sharp emission peaks observed in pure SAO at 650.9, 663.7, 689.8 nm disappear. Increasing ZnO from 5 to 15% and calcining them from 700 °C to 1200 °C, NBE as well as DBE peaks of ZnO emerge at the expense of the emission peaks of SAO and dominate over the emission of SAO. In SAO(20) composite, both NBE and DBE peaks become most prominent than all other composites. Further, we

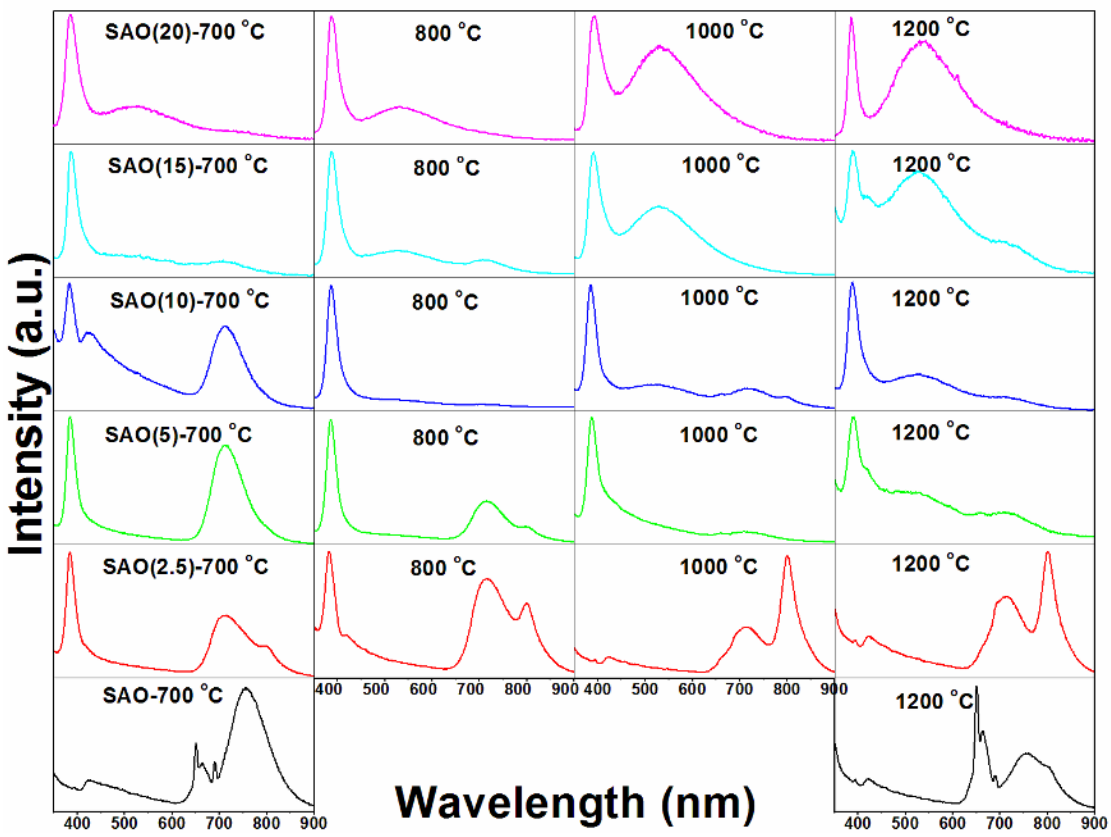

Figure 6.10: Photoluminescence spectra obtained by using Ex=266 nm for SAO(ZnO%) composites calcined at different temperatures in the range of 700–1200 °C.

demonstrate the PL spectra of SAO(20) composite calcined at four different temperature (700 to 1200 ^{o}C) in Fig. 6.11. A strong NBE peak at about 385 nm and a broad DBE emission band in the range of 440 to 800 nm is observed in all calcined samples. The emission spectra for 700 to 1200 ^{o}C calcined samples are deconvoluted and are shown Fig. 6.12. We have compared the DBE peak intensity of the composite calcined at different temperatures after normalizing the NBE emission peak intensity. It is found to be increased with increase in calcination temperature. The enhancement in defect band emission of ZnO clearly indicates that the excited electrons from the valency band of SAO and ZnO come back to the ground state by emitting photons only through the defect levels of ZnO. One may note an important observation in SAO(20) composite that the emission range covers the whole visible region. Fig. 6.13 shows the CIE colour space chromaticity diagram in two dimensional (x,y) coordinate

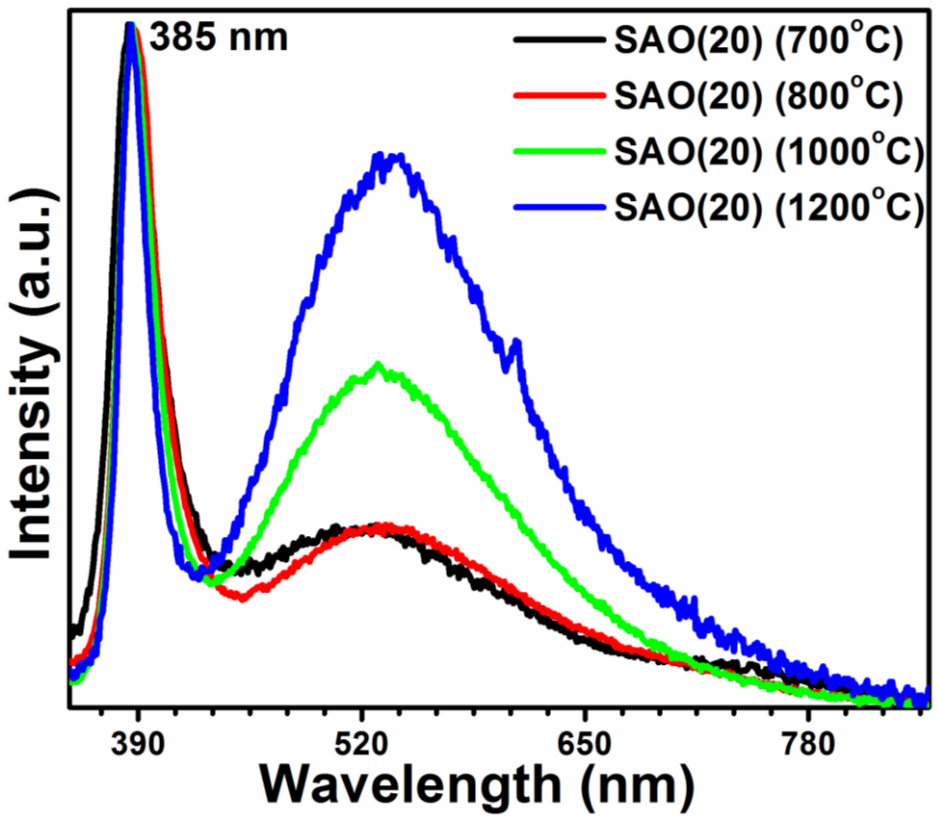

Figure 6.11: Photoluminescence spectra obtained by using Ex=266 nm for SAO(20) composites calcined at different temperatures in the range of 700–1200 ^{o}C.

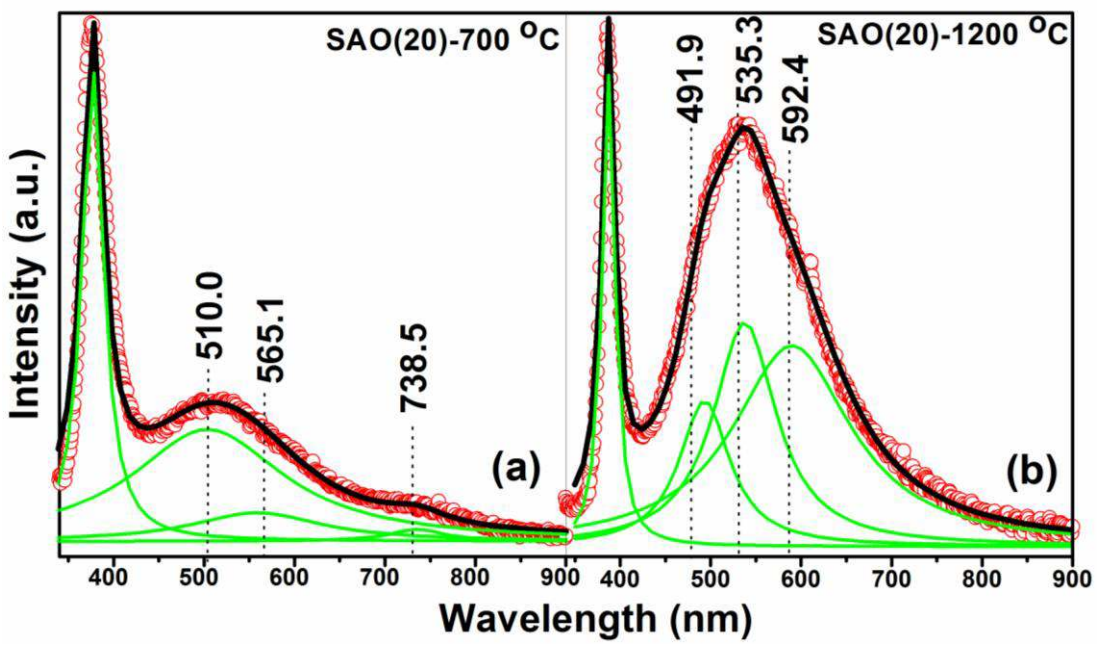

Figure 6.12: The deconvoluted spectra of SAO(20) composites calcined at **(a)** 700 °C and **(b)** 1200 °C.

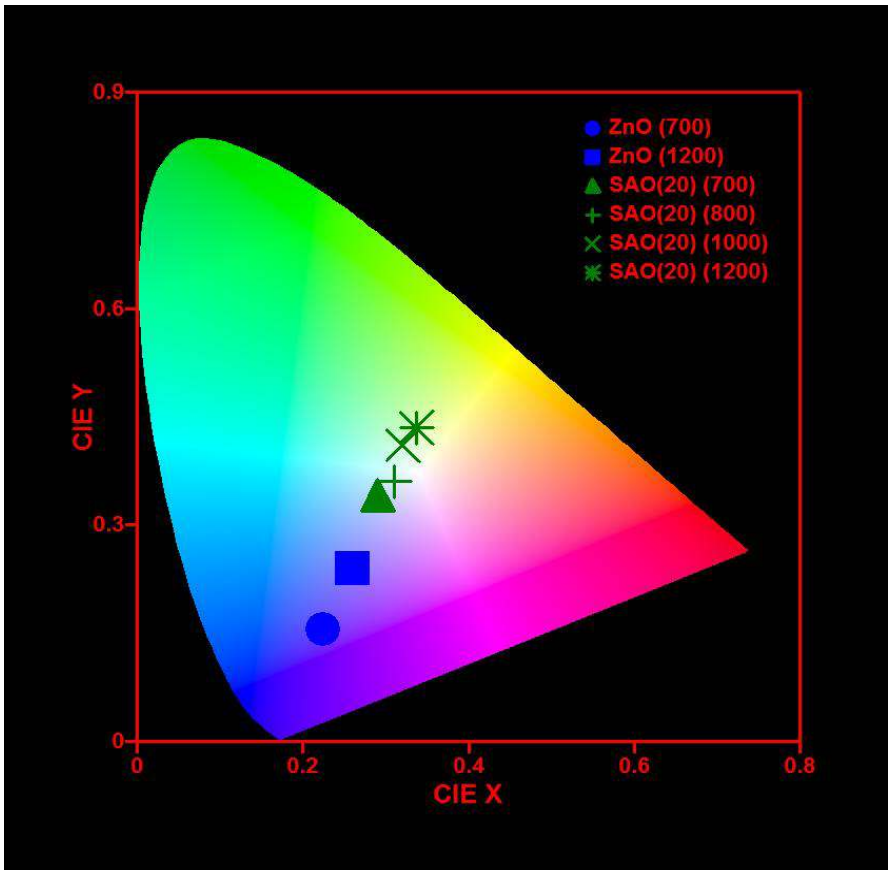

Figure 6.13: CIE chromaticity diagram of ZnO and SAO(20) composites calcined at different temperature.

system. The colour chromaticity coordinates are (0.22, 0.16), (0.26, .24), (0.29, 0.34), (0.31, 0.36), (0.32, 0.41), and (0.34, 0.44) for the samples ZnO (700 ^{o}C), ZnO (1200 ^{o}C), SAO(20) (700 ^{o}C), SAO(20) (800 ^{o}C), SAO(20) (1000 ^{o}C) and SAO(20) (1200 ^{o}C), respectively. The chromaticity coordinates of the composite calcined at various temperatures are very close to white light.

Further, the DBE band in SAO(20) calcined at 1200 ^{o}C becomes more intense at the expense of NBE peak after exciting with 355 nm laser source as shown in Fig. 6.14. The intensity ratio I_{DBE}/I_{NBE} is found to be increased from 0.808 to 2.014 after increasing the excitation wavelength from 266 to 355 nm in case of SAO(20) composite calcined at 1200 ^{o}C. We have carried out the excitation spectra with respect to the emission at 550, 600 and 655 nm and the results are shown along with the emission spectra in Fig. 6.14. Excitation

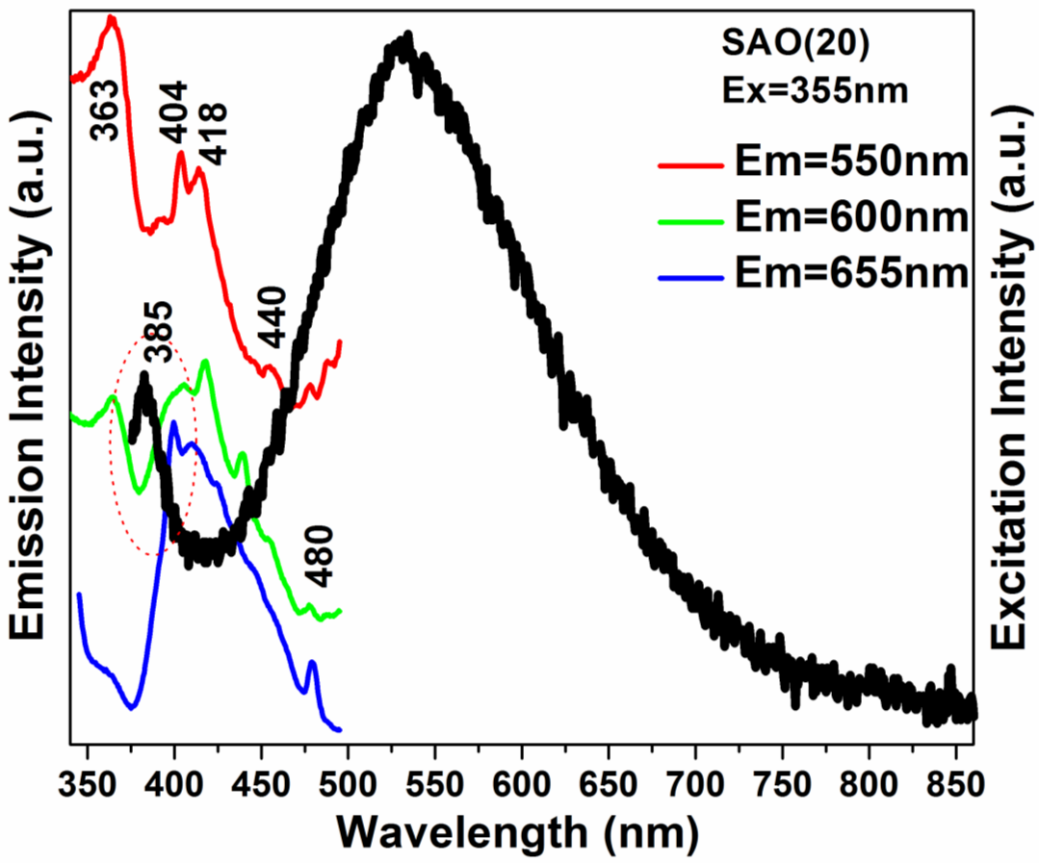

Figure 6.14: Photoluminescence spectra obtained by using Ex=355 nm for SAO(20) composites calcined at 1200 ^{o}C along with the excitation spectra for emission at 550, 600 and 655nm

spectra for emission at 550 nm demonstrate an intense band at 363 nm and few weak peaks at 404, 418, 440 and 480 nm. While the former bandconfirms the band-to-band excitation, the weak band confirms the excitation of electrons from VB to the intermediate defect states present in the band gap. The excitation spectra for emission at 600 nm shows increase in intensity of the band at 440 and 480 nm along with a decrease in the intensity of the band located at 363 nm. The excitation spectra corresponding to the 655 nm emission peak shows a less intense peak located at 363 nm and a broad band in the range of 375 to 490 nm accompanied with the peaks at 404, 418, 440 and 480 nm. Thus, from the excitation spectra corresponding to the emission monitored at 550, 600 and 655 nm, we confirm that the intensity of peak, responsible for NBE of ZnO, decreases and the intensity of the broad band above 385 nm increases which is responsible for DBE. Looking at the emission spectra obtained by using 266 and 355 nm excitation in case of SAO(20) composite calcined at 1200 ^{o}C, one may note that by exciting the sample with energy close to the band gap of ZnO (3.2 eV), more electrons relax through intermediate defect states of ZnO than direct band to band transition. The anomalous change in DBE peak in composites could not be explained considering the defect states of ZnO alone, because we have not observed any defect band emission either in ZnO calcined at 700 ^{o}C or 1200 ^{o}C excited with 266 nm energy source. Therefore, defect band emission corresponding to ZnO in composites is associated with the monoclinic/hexagonal phase of SAO having different native defects. The excited electrons from the defect states of SAO are deexcited through the defect states of ZnO emitting photons of energy in the range of visible region. The intensity of DBE band increasing in SAO(20) composite calcined at 1200 ^{o}C thus confirms more native defects. More native defects in monoclinic phase reported in literature is further confirmed from the PL data as shown in Fig. 6.12 [Wu *et al*. (2009); Dong-dong *et al*. (2000); Shafia *et al*. (2010)]. By exciting with 355nm, more electrons transfer their energy through the defect states of ZnO and hence defect band intensity in SAO(20) composite calcined at 1200 ^{o}C is enhanced.

Based on the photo luminescence data, we propose a tentative model to illustrate the mechanism of excitation and emission processes observed in SAO(20) composite calcined at 1200 ^{o}C in Fig. 6.15. In the band diagram, we have specified the energy level of V_{Sr}, V_{Al}, V_O, Sr_i, Al_i and O_i corresponding to SAO and V_{Zn}, V_O, Zn_i and O_i corresponding to ZnO. Exciting with photons of energy 4.66/3.49eV (266/355nm), electrons may show band to band excitation and the formation of excitons. Relative absorption processes of electrons are represented by A_1, A_2, A_3, A_4, A_5 and A_6 in the band diagram. Excited electrons are deexited directly to the valence band or trapped by the defect states of SAO (Sr_i, Al_i and V_O) and/or by defect states of ZnO (Zn_i, V_o, O_i and

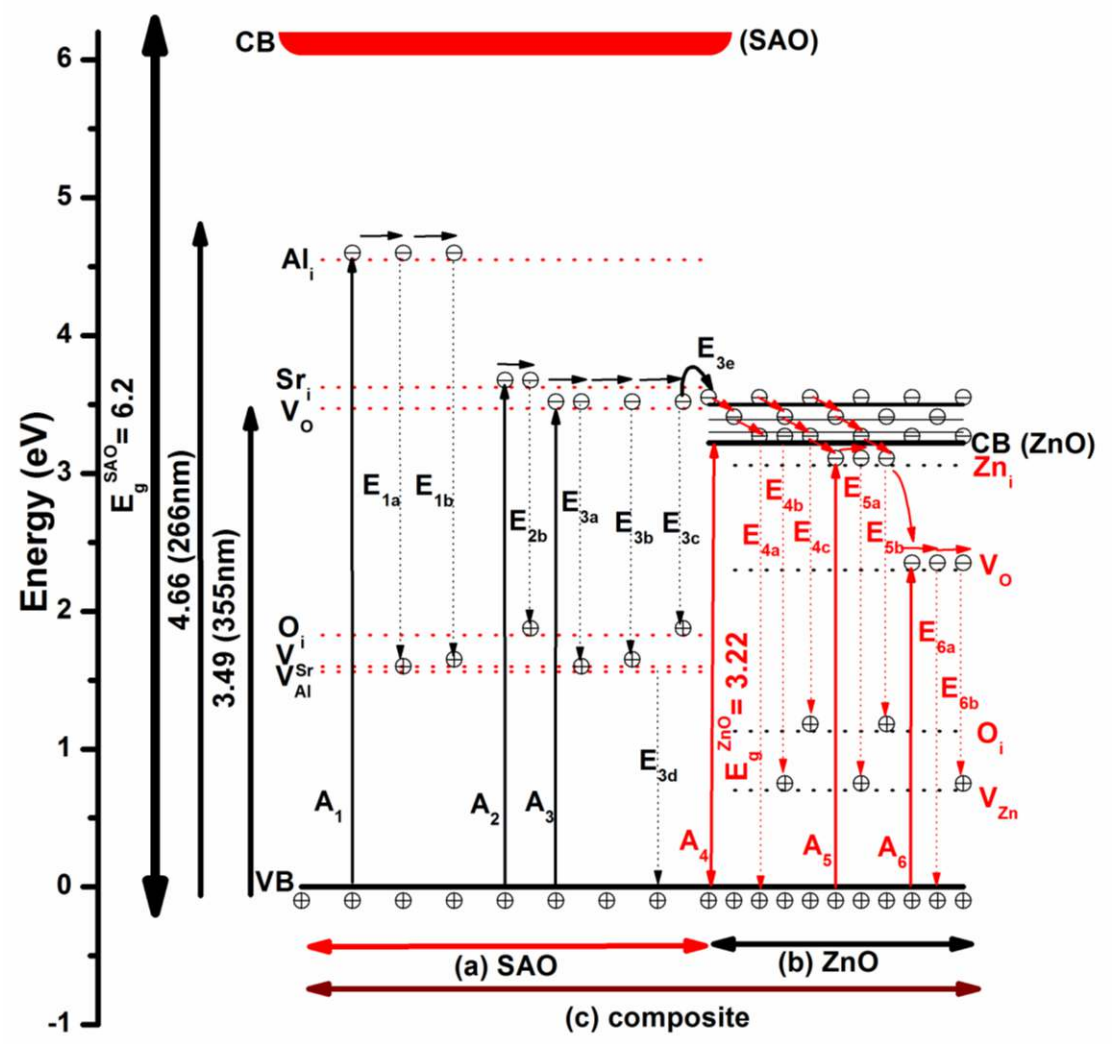

Figure 6.15: The proposed energy band diagram of the electron transfer in ZnO-SAO composites after excitation**.**

V_{Zn}). There could be a possibility of emission of electrons from donor levels Al_i, (emission processes are represented by $E_{1a,}E_{1b}$), from Sr_i(represented by E_{2a}) and from Vo (represented by E_{3a}, E_{3b} and E_{3c}) as there is evidence of emission peaks at 420 nm, 651, 664, 690, 755 nm in SAO observed by exciting at 266/355 nm. However, we do not find any emission peaks of SAO in SAO(20) composite calcined at 1200 ^{o}C. One may note that although there is a possibility of donor states of SAO to be populated by excitation of electrons, emission only occurs through the defect states of ZnO (process E_{3e}). This is only possible by transfer of energy from the donor levels of SAO to the lower energy levels of ZnO which includes the CB of ZnO and the deep defect levels such as Zn_i and V_O. The relative emission processes are E_{4a}, E_{4b}, E_{4c}, E_{5a}, E_{5b} and E_{6a}, E_{6b}. We conclude that intense white light emission is accompanied with the phase transition from hexagonal to monoclinic phase of SAO in presence of ZnO, is an important finding.

6.5 Thermoluminescence Study

Thermoluminescence (TL), a reliable technique to study defects, has been carried out in order to compare defects in SAO(20) composite calcined at 700 ^{o}C and 1200 ^{o}C, respectively. Fig. 6.16 (a-d) shows the TL spectra of composites before and after γ irradiation. A well resolved broad and intense single glow peak with maxima at ~323 ^{o}C is observed in the SAO(20) calcined at 700 ^{o}C. In addition to glow peak at ~323 ^{o}C, TL glow curve of SAO(20) calcined at 1200 ^{o}C exhibits one more peak with maxima at ~158 ^{o}C. The peaks observed at low temperature and high temperatures are denoted as peak-1 and peak-2, respectively. The maximum intensity observed for peak-1 and 2 at ~158 ^{o}C and ~323 ^{o}C denoted as T_{m1} and T_{m2}, respectively (Fig. 6.16). The intensity of peak-1 is very low compared to the peak-2 in SAO(20) calcined at 1200 ^{o}C. After irradiation with gamma (γ) rays, for a dose range of 15-75 Gy, the intensity of peak-1 in SAO(20) composite calcined at 1200 ^{o}C increases without changing the shape of glow curve. In contrary, the intensity and curve shape of peak-2 in both the samples does not show significant change in

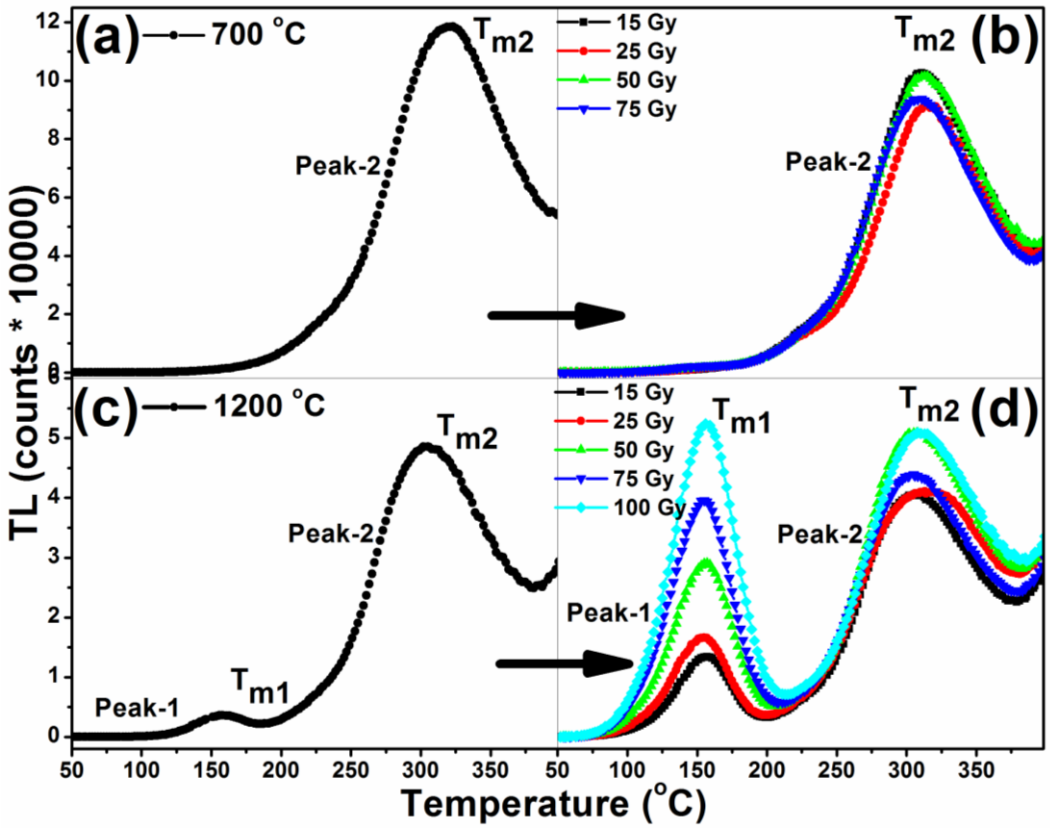

Figure 6.16: Thermoluminescence spectra of SAO(20) composite calcined at 700 °C and 1200 °C, before **(a and c)** and after **(b and d)** γ irradiation.

intensity even after increasing dose range. The increasing trend in intensity of peak-2 in SAO(20) calcined at 1200 °C, can be understood by the fact that more and more traps responsible for the glow peak, which are getting filled with electrons after increasing the irradiation dose. Afterwards, the trapped electrons annihilate with holes by thermal stimulation and gives rise to glow peak as observed in SAO(20) composite calcined at 1200 °C. It has been reported that electron traps are basically the lattice point defects which form during synthesis or heat treatment and create the charge noncompensation. So the electrons or holes can be trapped at these charge defects by the coulomb attraction [Raja *et al*. (2009)]. Thus it is confirm that SAO(20) composite calcined at 1200 °C with monoclinic phase has more defects than the SAO(20) composite calcined at 700 °C with hexagonal phase. It is noticed that T_{m1} and T_{m2}, do not change with increase in dose in both composites. This is a

characteristic of all first-order TL curves. From the first-order TL curves, depth of trap energy level in both composites can be calculated using the initial rise method [Bos *et al*. (2007)]. The formula for calculation is as follows:

$$I(t) = -\frac{dn}{dt} = \text{sn}\exp\{-\frac{E}{kT}\} \quad (6.1)$$

where, k is the Boltzmann's constant, the term *s* is called the frequency factor and *n* is for trapped electrons. Plotting ln(*I*) versus 1/*T*, a straight line is expected in the initial rise temperature range of glow peaks, from which the activation energy, *E* of trap is readily found. Using equation (6.1), from Fig. 6.17, activation energy, *E,* of trap for the SAO(20) composite calcined at 700 ^{o}C is found to be about 0.1840 $\pm$ 0.0044 eV corresponding to TL glow peak-2. Similarly from Fig. 6.18, activation energy for trap depths are calculated to be 0.0637 $\pm$ 0.0091 eV and 0.1628 $\pm$ 0.0270 eVcorresponding to the peak-1 and peak-2, respectively for SAO(20) composite calcined at 1200 ^{o}C. While same type of defect center are responsible for TL glow peak-2 in both the composites, new type of defect center emerges in SAO(20) composite calcined at 1200 ^{o}C with respect to the peak-1. The extra glow peak well corroborates with the enhanced DBE observed in composite accompanied with excess of native defects after calcination at 1200 ^{o}C. The total energy of defect free $SrAl_2O_4$ and $SrAl_2O_4$ containing V_O, V_{Al} or V_{Sr} defects are *ca.* -432, -430, -425 or -345 keV, respectively [T. Laamanen (2011)]. Thus, one may note that formation of V_{Sr} relatively needs high temperature. TL glow peak-2 in both the composites must be due to V_O which is present in both composites. However, peak-1 in SAO(20) composite calcined at 1200 ^{o}C may be attributed to V_{Sr} which appears due to the elevated calcination temperature, resulting in monoclinic phase. The increase in peak area or intensity of TL glow peak-1 in SAO(20) composite calcined at 1200 ^{o}C with irradiation dose may be applied in the field of radiation dosimeter. Fig. 6.19 shows the integrated peak area as a function of γ irradiation dose in the range from 0 Gy to 100 Gy corresponding to TL glow peak-1 of SAO(20) composite calcined at 1200 ^{o}C. The composite exhibits a remarkable linear dosimetric response in the dose range of 0 Gy

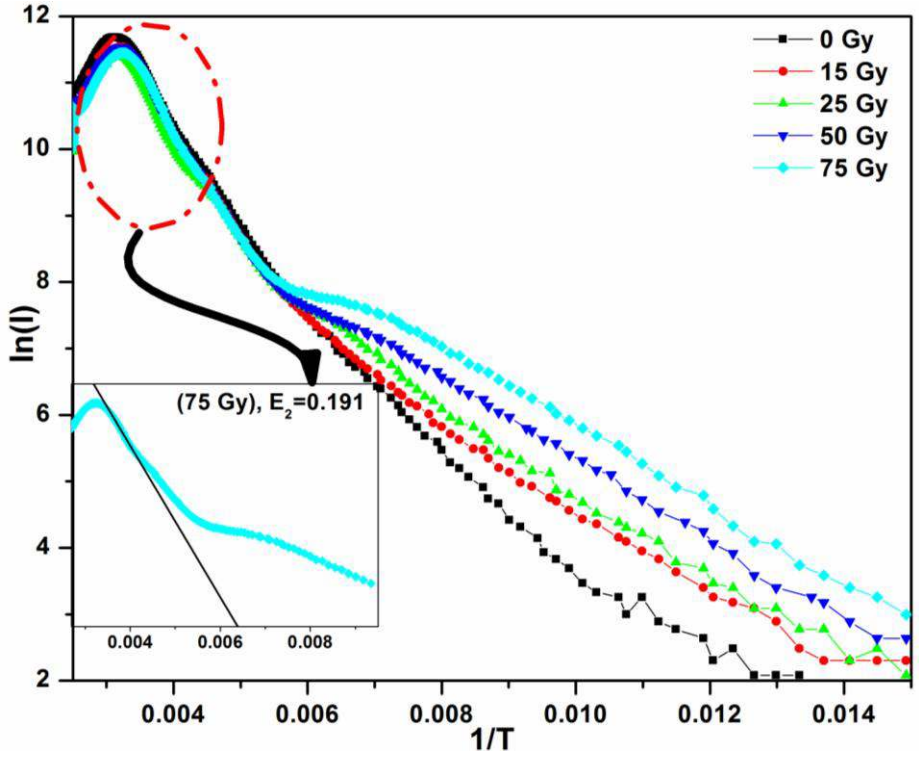

Figure 6.17: Calculation of activation energy *E* of traps for SAO(20) composite calcined at 700 °C with respect to the TL glow peak- at ~323 °C.

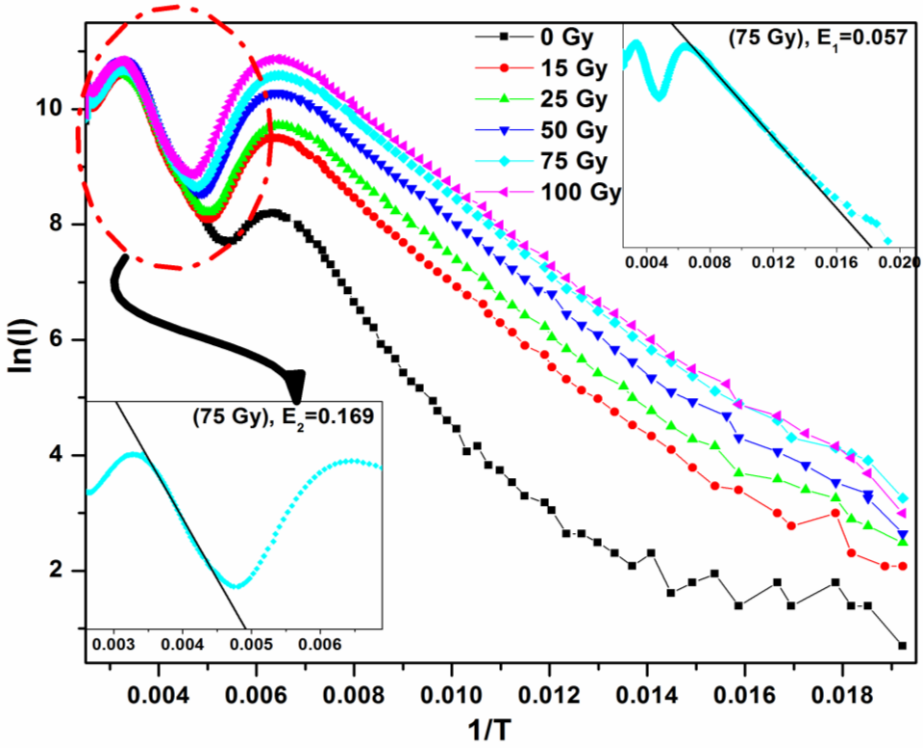

Figure 6.18: Calculation of the activation energy *E* of traps for SAO(20) composite calcined at 1200 °C with respect to the TL glow peak at ~323 °C and glow peak at ~158 °C.

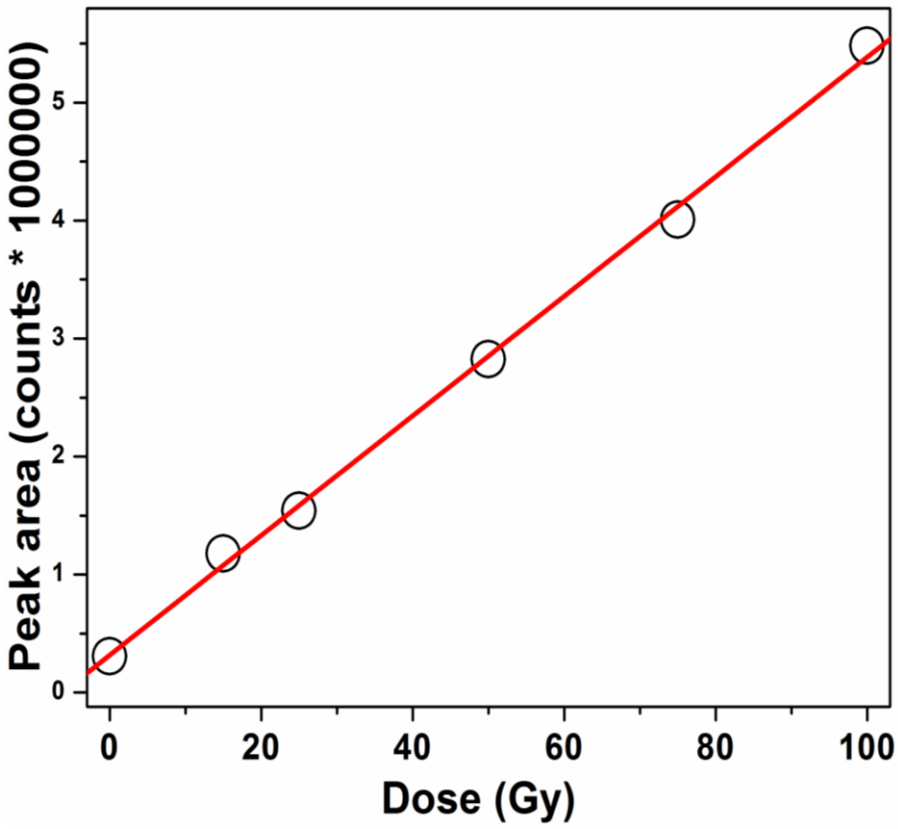

Figure 6.19: The linear response of integrated thermoluminescence of SAO(20) composite calcined at 1200 ^{o}C as a function of the γ irradiation dose with respect to the TL glow peak at ~158 ^{o}C.

to 100 Gy, which shows no indication of saturation response. For dosimeter applications, a linear dependence on the dose is highly desirable. Therefore, SAO(20) composite calcined at 1200 ^{o}C is found to be more suitable for the application of long lasting phosphor and may be explored for radiation dosimeter in future.

6.6 Conclusions

In this chapter, we showed that addition of ZnO was important in stabilising the high temperature hexagonal phase of SAO at room temperature. This could be possible by varying the concentration of ZnO in SAO synthesised through combustion technique. Monoclinic phase transformed to hexagonal by varying the concentration of ZnO from 2.5 to 20 wt% and further varying the calcination temperature from 700 to 1200 ^{o}C, hexagonal phase transformed to monoclinic phase. From photoluminescence study, it was

revealed that although a negligible broad green emission was observed in ZnO, in composite, with increasing calcination temperature, an increase in defect band emission of ZnO was observed. PL showed higher concentration of defects for monoclinic SAO in composite. TL study further confirmed the increase in number of defect centers in monoclinic phase compared to the hexagonal phase of SAO. We proposed an energy band diagram responsible for defect band emission observed in both the composites.